Monthly Notices of the ROYAL ASTRONOMICAL SOCIETY

MNRAS **497,** 192–203 (2020) doi:10.1093/mnras/staa1939
Advance Access publication 2020 July 7

Changing look active galactic nuclei in the MaNGA survey

Wei Jeat Hon,[1]★ Rachel Webster[1] and Christian Wolf[2]

[1]*School of Physics, University of Melbourne, Parkville, VIC 3010, Australia*
[2]*Research School of Astronomy and Astrophysics, The Australian National University, Canberra, ACT 2611, Australia*

Accepted 2020 June 20. Received 2020 June 3; in original form 2020 May 4

ABSTRACT

Changing look active galactic nuclei (CLAGNs) are rare cases of AGNs, where the continuum flux increases/decreases and the broad emission lines appear/disappear within short time-scales. These extreme changes challenge our understanding of accretion disc dynamics. We present a sample of four new CLAGNs at $0.026 < z < 0.107$, which were found by cross-matching the Mapping Nearby Galaxies at Apache Point Observatory (MaNGA) survey with AGNs from the SDSS spectroscopic data base. Our results show that the selection criteria of $> |0.5|$ mag change in SDSS-g band is ineffective at lower redshifts. This is, in part, due to the fact that the g band is probing a different part of the AGNs spectral energy distribution at these redshifts. The bigger issue is that the galaxy continuum dominates the spectrum and thus overwhelms any variation of the AGNs continuum that might contribute to photometric variations. This suggests the need to use different methods for future low-redshift CLAGNs searches.

Key words: galaxies: active – galaxies: emission lines – galaxies: general – galaxies: Seyfert – galaxies: supermassive black hole.

1 INTRODUCTION

Active galactic nuclei (AGNs) that undergo strong spectral flux changes of their broad emission lines are known as Changing Look AGNs (CLAGNs). These changes include the appearance or disappearance of broad emission lines [typically 'broad' is defined as Hβ and Hα of full width at half-maximum (FWHM) $> 2000\,\mathrm{km\,s^{-1}}$] as well as changes in the ultraviolet (UV)/X-ray spectral index or bolometric luminosity (Ruan et al. 2019). The time-scale for this change is unexpectedly short, ranging from months (e.g. Trakhtenbrot et al. 2019) to decades (Macleod et al. 2016).

CLAGNs have mostly been observed in low-luminosity Seyfert galaxies (Tohline & Osterbrock 1976; Penston & Perez 1984; Cohen et al. 1986; Bischoff & Kollatschny 1999; Denney et al. 2014; Shappee et al. 2014; Runco et al. 2016; Husemann et al. 2016), but more recently the phenomenon has also been found in low-luminosity quasars (LaMassa et al. 2015; Macleod et al. 2016, 2019; Ruan et al. 2016; Yang et al. 2018). This suggests the possibility that CLAGNs are preferentially lower luminosity AGNs.

The rate of the CLAGNs phenomenon is not well constrained. Systematic searches within the Sloan Digital Sky Survey (SDSS; Eisenstein et al. 2011) suggest that CLAGNs are rare. These searches select for CLAGNs through optical magnitude variability by imposing a $> |0.5|$ mag change threshold. They produce rates from ∼0.006 (Yang et al. 2018) to ∼0.03 per cent (Macleod et al. 2016, 2019, hereafter refer to these searches and Yang et al. 2018 as MC). However, this low rate can be attributed to their samples being selected from the SDSS-classified quasars without imposing a redshift or luminosity cut. Thus, their main sample is biased towards higher luminosity AGNs as these dominate the quasar sample in SDSS (Ross et al. 2013).

On the other hand, the CLAGNs rate is much higher in studies that are biased towards low-luminosity or low-redshift AGNs. Wolf et al. (2018) observed ∼3 per cent of CLAGNs out of 107 Seyfert galaxies at $z < 0.2$ using the same method as the MC searches but on the Hamburg–ESO Survey that is biased towards bright AGNs (Wisotzki et al. 1996). Runco et al. (2016) observed an even higher CLAGNs rate at ∼8 per cent[1] within a sample of 102 AGNs at $0.02 < z < 0.1$. A difference in their work is that every AGN was inspected, instead of applying a selection cut on magnitude variability, which avoids excluding CLAGNs without observable variability. Therefore, the focus of this work is to inspect an even larger unbiased sample of low-luminosity, low-redshift Seyferts in SDSS.

The Mapping Nearby Galaxies at Apache Point Observatory (MaNGA) is a integral-field spectroscopic survey that targets 10 000 nearby galaxies at $0.01 < z < 0.15$ (Bundy et al. 2015). Its parent catalogue is the NASA–Sloan Atlas, which contains galaxies with a completeness of up to 98.6 per cent. At the time of the SDSS Data Release 15 (Aguado et al. 2019), MaNGA contained 4621 unique galaxies. The MaNGA sample is selected to have a roughly flat distribution in $\log_{10}$(total star mass) and thus prefers more massive galaxies relative to their true cosmic fraction (and references therein Wake et al. 2017). Since the fraction of galaxies hosting AGN increases with stellar mass (Kauffmann et al. 2003), Seyfert galaxies and, consequently, CLAGNs are expected to be well represented

[1]Runco et al. (2016) quotes a rate of 38 per cent for AGNs that had a classification change, but most of these are minor classification changes that are not typically considered as CLAGNs.

★ E-mail: whon@student.unimelb.edu.au

in the MaNGA survey (Seyfert galaxies discoveries in MaNGA: Wylezalek et al. 2018; Nascimento et al. 2019, among others).

In this paper, we present the first comprehensive search for CLAGNs in the MaNGA sample. We define CLAGN as an AGN that undergoes a change in AGN type as determined spectroscopically. The commonly used classification scheme by Osterbrock (1981) includes types 1, 1.2, 1.5, 1.8, 1.9, and 2, as well as a fainter subclass of AGNs known as low-ionization nuclear emission-line regions (LINERs). The main AGN types primarily depend on the flux ratio of the broad H β and H α emission lines. However, it is common practice in CLAGN studies to amalgamate types 1.2 and 1 into type 1 s, as well as types 1.8 and 1.5 into type 1.5 s. Changes within the amalgamated types are considered less significant. In this scheme, AGN with both broad H β and H α are type 1, and those without either are type 2. Those with only broad H α are type 1.9, and those with a 'weak' H β are type 1.5. The strength of the broad H β line is quantified by comparing it to the narrow H β line or the [O III] line that is typically present in a Seyfert galaxy and not expected to vary on CLAGN time-scales. A broad H β line is considered 'weak' when its flux is comparable to the narrow component. We use $F_{\mathrm{H}\beta,\,\mathrm{broad}}/F_{\mathrm{H}\beta,\,\mathrm{narrow}} < 10$ that is empirically shown to describe type 1.5 AGN in a small sample (Cohen 1983). When narrow H β is not present, we use $F_{\mathrm{H}\beta,\mathrm{broad}}/F_{[\mathrm{OIII}]} < 1$ since usually $F_{[\mathrm{OIII}]}/F_{\mathrm{H}\beta,\mathrm{narrow}} > 3$ in an AGN.

LINERs are AGNs that are dominated by narrow emission lines of low ionization. Changing Look LINERs have been reported by Frederick et al. (2019), however, the flux changes of the broad lines that are measured are similar to CLAGN in the main AGN types. Therefore, for the scope of this paper, we will not place a strong emphasis on the distinction of LINERs. The paper is structured as follows: Section 2 describes our sample selection and CLAGNs search method. Section 3 presents our CLAGNs findings, including spectra, light curves, and line-fitting measurements. Section 4 discusses the CLAGN we found and some AGN with other significant changes. Section 5 is a summary. We adopt a flat cold dark matter λcold dark matter (ΛCDM) cosmology with $\Omega_\Lambda = 0.6847$ and $H_0 = 67.36\,\mathrm{km\,s^{-1}\,Mpc^{-1}}$ (Aghanim et al. 2018).

2 DATA AND SEARCH FOR CLAGNS

We perform a search with minimal cuts applied to the sample by comparing the MaNGA and SDSS spectra and determining significant broad emission-line changes, both qualitatively and quantitatively.

The MaNGA data were accessed through CASJOB,[2] where we found 11 370 non-unique entries in the full data base. We reduce this to an AGN sample of 438 unique objects by requiring that the SDSS spectrum has type values of GALAXY, QSO, or AGN in the columns SPTYPE and SPCLASS, and the class values including AGN or BROADLINE in the column SUBCLASS. We include both SDSS spectra taken from the SEGUE (Yanny et al. 2009) and BOSS (Dawson et al. 2012) instrument (hereafter referred to SDSS and BOSS spectrum).

We extracted the (one-dimensional) 1-D spectra from the MaNGA Intergral Field Unit (IFU) data cubes using QFitsView.[3] The data cubes are arranged in square arrays of spaxels with 0.25 arcsec^2 area and have one wavelength dimension. The circular apertures used in QFitsView for spectral extraction select an approximately circular shape built from full spaxels. Emulating the circular fibre apertures of SDSS would require using fractional spaxels around the perimeter of the aperture. SDSS and BOSS use fibre diameters of 3 and 2 arcsec, respectively, which translate into fibre areas of 7.07 and 3.14 arcsec^2 (Yanny et al. 2009; Dawson et al. 2012).

Aperture differences impact the mixing of stellar and nuclear light. Therefore, apertures used for extraction of MaNGA spectra in QFitsView must be as similar as possible to the original fibre areas in SDSS and BOSS. We use 29 and 13 pixel apertures for objects with SDSS and BOSS spectra, respectively, which correspond to areas of 7.25 and 3.25 arcsec^2. The differences are thus negligible for the purposes of this paper, where we aim to detect major type changes.

SDSS and BOSS spectra were accessed through the Science Archive Server.[4] We normalize all spectra to their average continuum level between 5200 and 6200 Å in rest wavelength. We then divide the pair of MaNGA and SDSS spectra of each object to detect signatures of changes in the H β and H α broad-line flux (examples presented in the Appendix). Signatures of changes are any features in the divided spectrum that deviates from the mean (typically unity). We discard objects without any features or with only narrow line features in H β and H α. Determination of narrow line features was done by comparison with SDSS templates.[5] We overlay the 'late-type galaxy' template on the divided spectrum and visually gauge the similarity (see examples in the Appendix). We checked the spectra of the remaining objects to ensure the changes are not due to noise or artefact. Using this method, we find nine objects out of our sample of 438 MaNGA AGN that exhibit strong variations in H β and H α broad-line flux.

To further quantify these changes, we use the PYTHON package PPXF (Cappellari 2016). Here, we fit a Gaussian (mean, standard deviation, and weights as initial parameters corresponding to location, width, and height of the feature) to the H β and [O III] emission line in a section of the spectrum, while the continuum is fitted with a low-order polynomial. From the fitting, we derive the centroid from the fitted mean of the Gaussian, line flux by integration, and the FWHM accordingly. In some cases, multiple Gaussian curves were required to fit an emission feature. For these, we add them together and derive the centroid from resulting mean of the curve, while deriving the flux and FWHM the same way. The properties of the Gaussian fits were restricted to be positive for emission lines with a FWHM $< 1000\,\mathrm{km\,s^{-1}}$ for narrow lines, a $1000 < \mathrm{FWHM} < 2000\,\mathrm{km\,s^{-1}}$ for intermediate lines, a $2000 < \mathrm{FWHM} < 5000\,\mathrm{km\,s^{-1}}$ for broad lines with a Gaussian centroid drift from the laboratory wavelength <100 Å.

The final value for the flux is an average over nine line-fitting results using a polynomial of order 1, 2, and 3, each wavelength ranges of 4400–5500, 4500–5600, and 4400–5400 Å. The greatest uncertainty measured using this method was 5 per cent. We also consistently find a deviations of less than 5 per cent in the chi-squared test, FWHM, and centriod, which is tolerable for our purpose of identifying strong line flux changes. We tested the significance of each fitted Gaussian curve by comparing the Chi-squared statistics with and without it.

The search resulted in the identification of four new CLAGN candidates: J0828427+454433, J1118032+450646, J1126377+513423, and J1605051 + 452634. We present their MaNGA and SDSS or BOSS spectra in Fig. 3. The remaining five, whilst exhibiting strong broad-line variations, did not fit the typical CLAGN requirement for type classification changes (refer to them as 'supplementary sample',

[2] https://skyserver.sdss.org/CasJobs/
[3] https://www.mpe.mpg.de/~ott/QFitsView/
[4] https://dr12.sdss.org/ Spectra from data release 15 are accessible from here
[5] http://classic.sdss.org/dr5/algorithms/spectemplates/

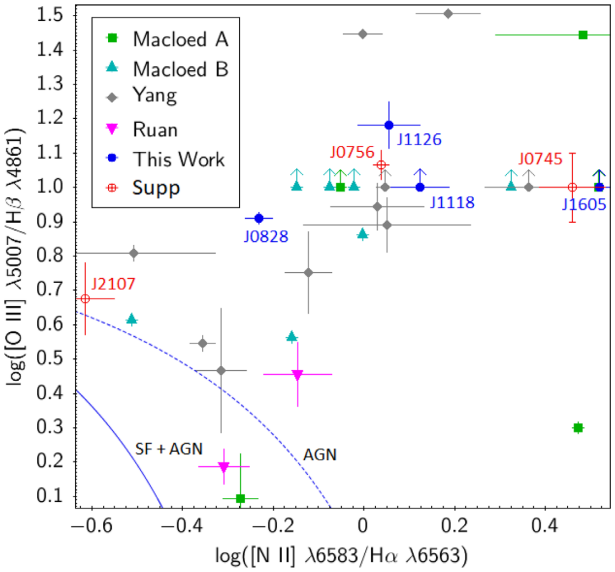

Figure 1. BPT diagram with Hβ, Hα, [OIII], and [NII] lines. We include CLAGN from this work, MC (Macleod A, Macleod B), Ruan et al. (2016), MC, and three from the supplementary sample. Solid blue line is from Kauffmann et al. (2003) and separates composite AGN from star-forming galaxies. Dotted blue line is from Kewley et al. (2001) and separates AGN from composite AGN. All presented CLAGN are AGN according to this classification scheme. We do not include the remaining two objects from the supplementary sample as their emission features are much more complex and fitting results may be arbitrary.

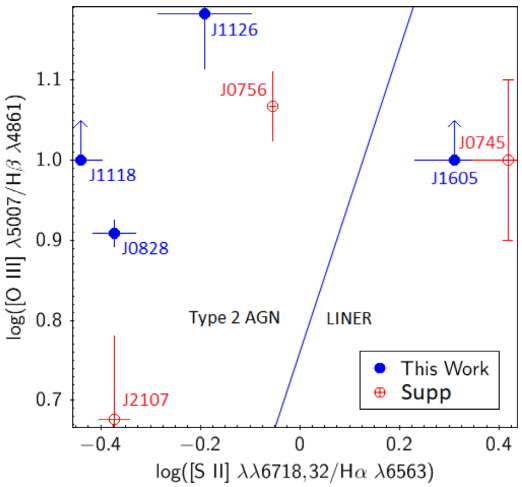

Figure 2. BPT diagram with Hβ, Hα, [O III] and [S III] lines. We only present CLAGNs from this work and also the variable objects from the supplementary sample. Error bars are identical to Fig. 1. Blue line is from Kewley et al. (2006), separating Seyfert 2 AGN on the left-hand side and LINER galaxies on the right-hand side.

spectra presented in Figs 4 and 5). None the less, they exhibit strong variations and we discuss them in Section 4.2.

To confirm that the four CLAGN candidates are AGNs, we also perform line fitting on the Hα region for the bright phase spectra to obtain line ratios for a BPT diagram analysis with the BPT classification from Kauffmann et al. (2003) and Kewley et al. (2001). Line ratios of interest are the narrow line ratios of [O III]/Hβ, [N II]/Hα, and [S III]/Hα. This is shown in Figs 1 and 2. For comparison, we also calculate line ratios for the known CLAGNs from the MC searches and Ruan et al. (2016) that have an Hα emission region within the spectral range. CLAGNs with an unresolved narrow line are excluded. For CLAGNs with two accessible spectra, which includes our objects, the mean value from the two spectra is used and the variation or spread of their values becomes the systematic error. The variation of the object dominates the 5 per cent measurement uncertainty, which results in much larger error bars. In some cases, the narrow Hβ line is unresolved or undetected. For these, we assume a lower limit of $\log([\mathrm{O\,III}]/\mathrm{H}\beta) = 1$ and they are presented with an arrow above their points. Since these objects are highly likely to be AGN based on their x-axis position in Fig. 1, the actual y-axis value is not important. J0745072+460420 does not have Hβ and [O III] emission lines therefore no y-axis data. We indicate this object with a capped error bar on both ends. BPT diagnostics from the figure indicates that our objects are confidently AGNs.

3 RESULTS

3.1 New CLAGN and change rate

As presented in Fig. 3, J1118032+450646, J1126377+513423, and J1605051+452634 are turn-on CLAGN given that a broad Hβ emission line appeared in the newer MaNGA spectrum; J0828427+454433 is a turn-off CLAGN as the broad Hβ line from the older BOSS spectrum has disappeared in the MaNGA spectrum. Table 1 presents the line-fitting results, derived type based on the definition in the Introduction, broad Hα emission luminosity, redshifts, and coordinates. Fig. 3 presents the spectra and relative-change plots of all four CLAGNs. The MaNGA spectra are re-binned to the lower wavelength resolution of the SDSS spectra and smoothed with a Gaussian to be visually identical in the narrow-line profile. The relative-change plots are constructed from the continuum-subtracted spectra normalized to the [O III] (5007 Å) flux. This scaling is done by setting the peak of Hα to the value of the percentage change of Hα broad-line flux. The aim of this scaling is to illustrates visually how much the spectra differ.

We also found that some of the 438 objects in the original sample are not AGNs, but were mistakenly classified by an automated classifier used in SDSS.[6] Here, we do not determine an exact number of AGNs within the sample as classifying AGNs is beyond the scope of this paper. With four CLAGNs among less than 438 true AGNs, we find a lower limit to our CLAGNs rate of $\sim$1 per cent. As expected, this rate is in the same order as the 3 per cent rate found by Wolf et al. (2018) and much higher than those found in MC searches. This suggests that the selection method employed in this study finds a larger percentage of CLAGNs than some of the earlier published methods.

3.2 Magnitude variability

We now ask whether these four newly found CLAGNs would have been detected using a selection method requiring >0.5 mag change in optical magnitude (MC searches, e.g. MC). Such a change is mainly caused by changes in the optical continuum luminosity from an accretion disc, while the emission lines usually make a minor contribution. Answering this question in retrospect requires that there is photometry for epochs close to the date of the spectra to enable a comparison. This is not the case for our CLAGNs. SDSS photometry

[6]Examples of wrong SDSS classification: SDSS J015244.40+131133.3, J151256.88+301816.3, J140737.16+442856.2

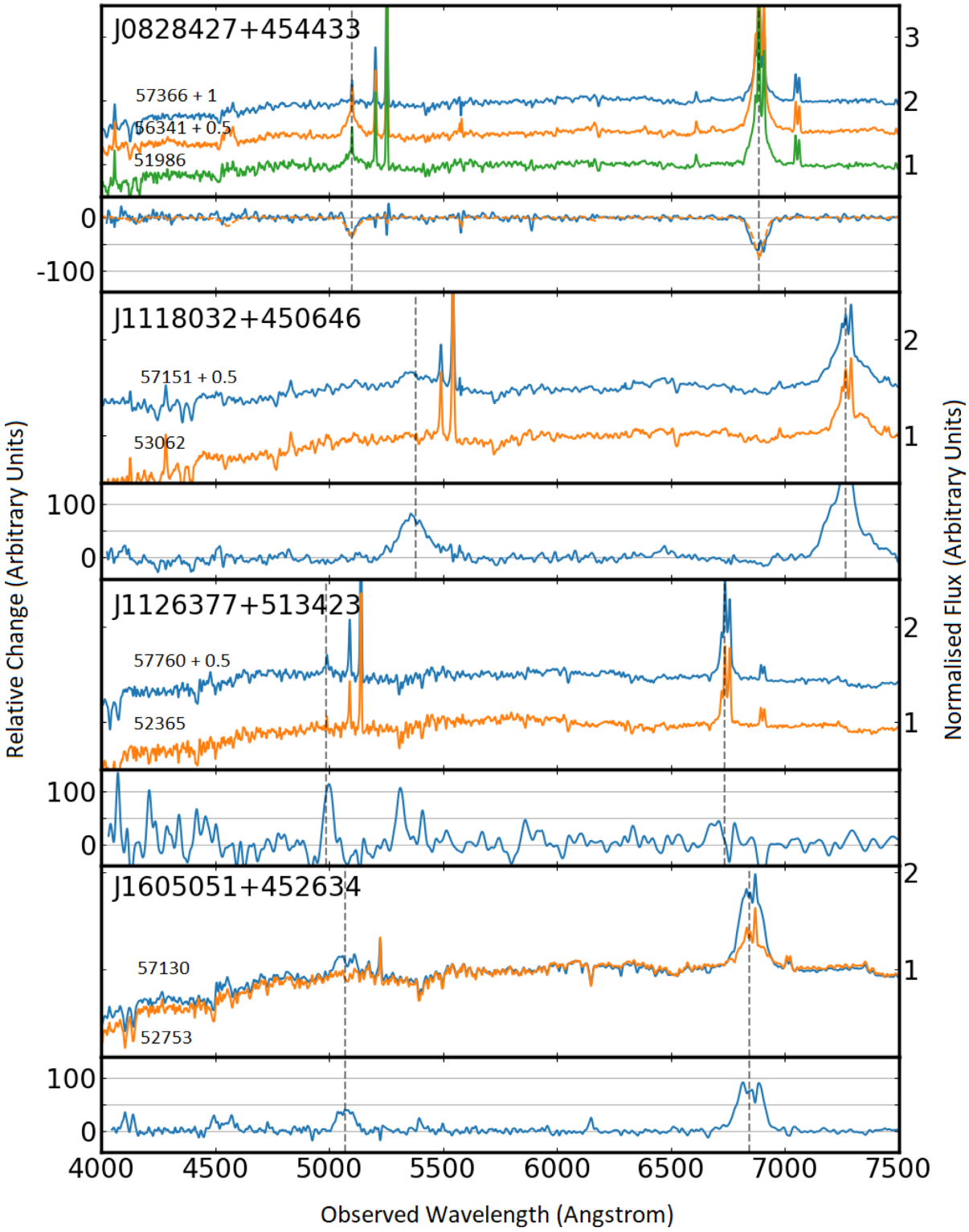

Figure 3. New CLAGN: Top panels show new spectra from MaNGA (blue) versus older spectra from SDSS (orange), both normalized with respect to [O III] line flux. J0828427+454433 also has a BOSS spectrum (green). Bottom panels are relative-change plots showing the MaNGA/SDSS ratio with horizontal lines across depicting the percentage of changes. J0828427+454433 has an additional line for the MaNGA/BOSS ratio. For clarity, spectra are vertically offset, ordered in time and labelled with Modified Julian Dates (MJD). Vertical dashed lines mark the laboratory wavelength of H β and H α.

exists 1 yr prior to the time the SDSS spectra were taken. For the epochs of the MaNGA spectra, we can useAll Sky Automated Survey for SuperNova (ASAS-SN; Kochanek et al. 2017), the Catalina Sky Survey (CSS, Drake et al. 2009), and the Palomar Transient Factory (PTF, Law et al. 2009). However, each of these facilities uses different filters and aperture sizes compared to SDSS. While

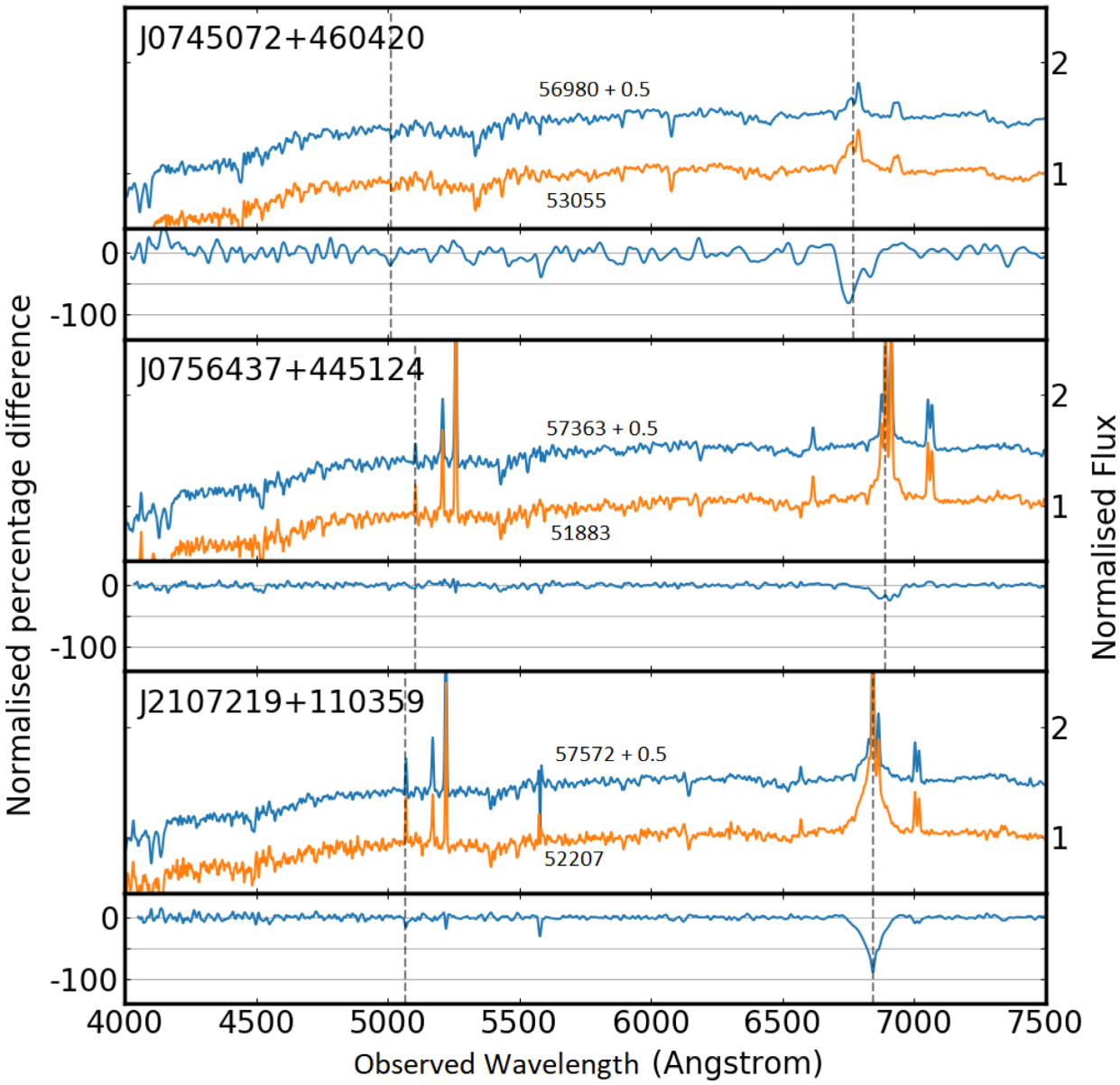

Figure 4. Other objects: figure style as in Fig. 3. For the relative-change plot of J0745072+460420, we normalized to the mean between 5500 and 6500 Å instead, because the [O III] line is absent.

colour and aperture transformations are possible in principle, due to their complexity, their assumptions mean that they are highly uncertain and we do not attempt them here. Therefore, we are unable to assess the viability of the selection method for our CLAGNs. None the less, studying the light curves and variability is still informative.

In addition, we consider mid-infrared (MIR) data (profile-fit magnitudes `mpro`) from *WISE* and *NEOWISE* (hereafter just referred to as *WISE*; Wright et al. 2010; Mainzer et al. 2011), because MIR variability is expected and observed in some CLAGNs (MC; Sheng et al. 2017; Stern et al. 2018).

We also checked the available Pan-STARRS1 (Flewelling et al. 2019) photometry for our objects and found it was not conclusive. While Pan-STARRS1 provides excellent stacked mean epoch photometry, it lacks temporal coverage. We have attempted to create light curves by binning single-exposure photometry within 100 d. The light curves then show variability, but such variability is also observed in nearby non-varying stars and non-AGNs galaxies at similar redshift, size, and brightness, which are not expected to vary intrinsically at the observed rate.

Fig. 6 presents light curves from ASAS-SN, CSS, and *WISE*, which are constructed by averaging measurements within time bins of 50 d to reduce systematic errors. We also apply iterative 3σ cuts to the FWHM associated with the magnitude measurements for each light curve. Both ASASN-SN and CSS light curves effectively contain total galaxy photometry. ASAS-SN uses a 16-arcsec aperture photometry in V and g bands, while CSS uses V band photometry with apertures matched to the size of the host galaxy. PTF provides Kron aperture photometry in g band, and is only shown for objects where we found more than two epochs. Also note that PTF contains sets of measurements that are not always consistent with one another, often deviating by more than 0.5 mag at the same epoch. Therefore,

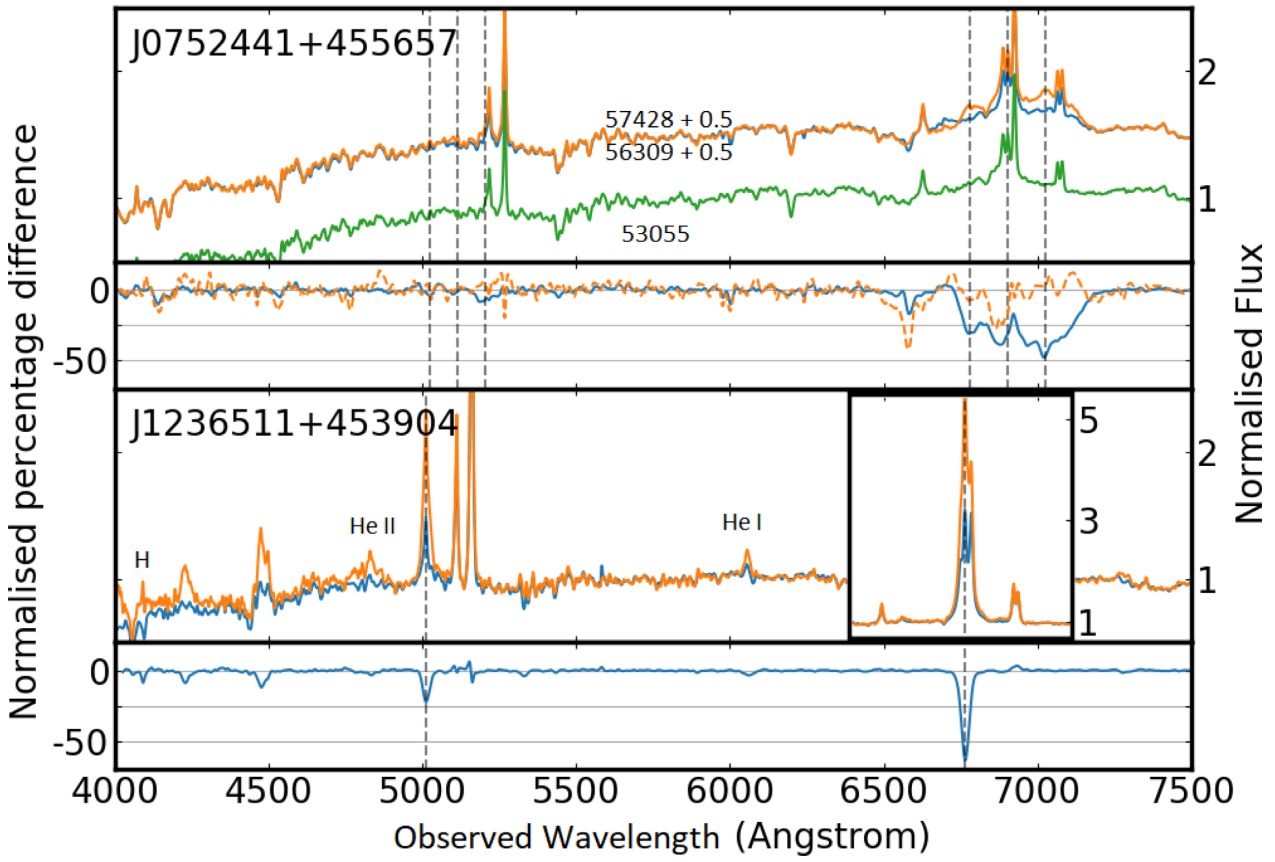

Figure 5. Unusual objects: figure style as in Fig. 3. For J0752441+455657, the MaNGA spectrum (blue) has weaker H α broad emission lines. We also show the redshifts for the red- and blue-ward troughs. For J1236511+453904, the MaNGA spectrum (blue) has weaker emission lines overall. We indicate the H absorption, He II and He I emission features. The snippet is showing the full scale of the H α region. We separated the H α region for this plot such that the rest of the spectrum can be shown in better detail. Note that we halve the scale on the relative-change plots for the same reason.

Table 1. Line flux ratios and inferred types of the four CLAGNs. Missing entries denote emission features that are non-existent or not detected in our analysis. MaNGA column for J0828427+454433 is the line-fitting results from the spectrum extracted with the aperture of 2 pixel radius that is closest to BOSS spectrum. Other objects will have line-fitting results from the 3 pixel radius aperture. Percentage broad H α differences are absolute percentage variations calculated based on the luminosity values of the specified spectrum and MaNGA.

	J0828427+454433			J1118032+450646		J1126377+513423		J1605051+452634	
	SDSS	BOSS	MaNGA	SDSS	MaNGA	SDSS	MaNGA	SDSS	MaNGA
MJD	51986	56341	57366	53062	57151	52365	57760	52753	57130
$F_{\mathrm{H}\beta,\mathrm{narrow}}/F_{[\mathrm{OIII}]}$	0.094	0.120	0.127	–	–	0.058	0.075	–	–
$F_{\mathrm{H}\beta,\mathrm{broad}}/F_{[\mathrm{OIII}]}$	0.423	0.750	–	–	1.159	–	0.335	–	6.135
$L_{H\alpha,\,broad}(10^{40}ergs/s)$	9.201	12.357	2.03	64.656	87.522	1.061	1.14	13.537	21.727
$\Delta L_{\mathrm{H}\alpha,\,\mathrm{broad}}$	83.6 per cent	77.9 per cent		35.36 per cent		7.49 per cent		60.51 per cent	
$F_{\mathrm{H}\beta,\,\mathrm{broad}}/F_{\mathrm{H}\beta,\,\mathrm{nw}}$	4.482	6.251	–	–	–	–	4.491	–	–
Derived type	1.5	1.5	1.9	1.9	1.5	1.9	1.5	1.9	1
Redshift		0.0491		0.1072		0.0264		0.0433	
RA, Dec.		127.1779, 45.7425		169.5133, 45.1128		171.6571, 51.5731		241.2712, 45.4428	

we only choose to present a set that has the most epoch coverage. In the following sub-sections, we discuss the photometry and spectral variability for each of our objects individually.

3.2.1 J0828427+ 454433

This object has three spectra separated by 11.9 and then 2.8 yr, with types classifications of 1.5, 1.5 , and 1.9 in order of epoch. Between the BOSS and MaNGA spectra, the broad H β line has disappeared and the broad H α luminosity has decreased by ∼80 per cent. We note that a significant portion of the variation between the SDSS and BOSS spectra is likely due to the dissimilar fibre diameter. Since the relative-change plots of both MaNGA/SDSS and MaNGA/BOSS are almost similar, we can conclude that there was little variation between SDSS and BOSS spectra.

Among the light curves, we only find variability in *WISE* bands, where the object dims by ∼0.7 mag around the last two spectral epochs. This is consistent with the observed loss of broad emission lines in the spectrum (see Fig. 3); as the accretion fades in a turn-off CLAGN, we expect both the excitation source for broad lines and the

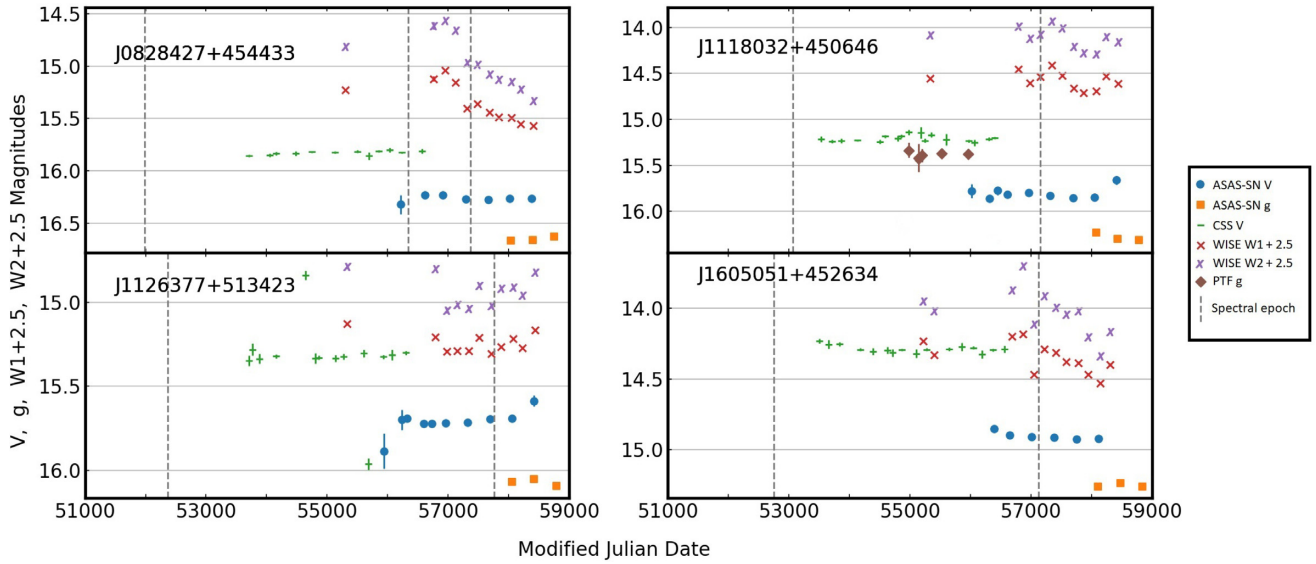

Figure 6. Optical and MIR light curves of our CLAGNs. *WISE W1* and *W2* is offset by 2.5 to fit in the same scale. Magnitude uncertainties are shown as error bars but are often too small to be visible. Horizontal lines are included to help indicate magnitude changes of >0.5 mag. Note that full references and data sources are presented in Section 3.2.

heating source for nuclear dust clouds to vanish. Interestingly, we do not observe any variability in the optical light curves, which might be due to large apertures diminishing the contribution of the nuclear signal. Hence, this object would not be detected as a CLAGN from the available optical photometry.

3.2.2 J1118032+450646

The spectra of this object were taken 11.2 yr apart, changing from type 1.9 to 1.5. In the MaNGA spectrum, a broad H β line has emerged and the broad H α luminosity has increased by ∼35 per cent. Most of the light curves show modest variability, but none of which are characteristic of a CLAGN, i.e. strong changes between bright and dim stages.

The Catalina Real-Time Transient Survey (CRTS) light curve has a ∼0.15 mag increase between MJD 54500 and 55500. It is possible that the CLAGNs event occurred during this time frame, and the weak response in the light curve is due to host dilution from a larger aperture. However, we do not have a spectrum around that time frame to confirm its relation to the CLAGNs event. *WISE* light curves, on the other hand, are oscillating with an amplitude of ∼0.2 mag, which is rather puzzling. Meanwhile, the ASAS-SN *V* suggests a brightening after the MaNGA spectrum, although this might not be the case as it contradicts the ASAS-SN *g* light curve. We encourage a spectral monitoring effort to verify the evolution of this object.

3.2.3 J1126377+513423

The spectra of this object were taken 14.7 yr apart, changing from type 1.9 to 1.5. Between the spectra, a weak broad H β line appeared, while the broad H α luminosity increased by 7.5 per cent. These are much weaker changes than in other known CLAGNs, however, we still count the object in the CLAGNs category because its Seyfert type changes from 1.9 to 1.5.

We also observe only weak optical variability, but do not have data going far enough back in time to cover the first spectral epoch. However, the acute increase in ∼0.2 mag around 56000 MJD could be the beginning of the changing event and suggests a changing time-scale of ∼5 yr, but there is no spectral data at the time to show this. Since the *W1*, *W2*, and *V* band light curves are still increasing after the MaNGA spectrum, we expect that future spectra may show stronger broad lines.

3.2.4 J1605051+452634

The spectra of this object were taken 12 yr apart, changing from type 1.9 to 1. It is considered a LINER AGN, according to the BPT in Fig. 2, due to the much weaker H α and H β emission lines compared to [S III]. Between the spectra, a broad H β line appeared and the broad H α flux increased by ∼60 per cent. None of the optical light curves exhibit significant variability.

W1 and *W2* started to dim around the epoch of the MaNGA spectrum consistent with the small decrease in ASAS-SN *V*, and then dropped by ∼0.5 mag over 200 d. We hypothesize that it could be accompanied by a disappearance of at least the broad H β line and perhaps a substantial weakening of H α. We encourage observation of newer spectra to reveal any recent type changes back to ∼1.9.

4 DISCUSSION

4.1 Insights from our CLAGNs

Except for J0828427+454433, we do not have sufficient coverage of optical magnitude measurements or spectral data for the light curves to provide any addition information. Having such a large gap in time between spectra is problematic. For example, in the case of J1126377+513423, the optical variation is meaningless since we cannot be sure if it is related to the Changing Look event without at least two spectra around the epoch.

We also find little evidence of any optical magnitude variability at the 0.5 mag scale in our light curves. This is most significant in the case of J0828427+454433, where we expect a decrease in magnitude between the BOSS and SDSS spectra due to the loss of broad emission lines. We checked both CSS and ASAS-SN for known CLAGNs light curves, but there is only a handful of CLAGNs with timely measurements in these data base and hence the data is

inconclusive. While Trakhtenbrot et al. (2019) reported a redshift 0.017 CLAGNs with a ASAS-SN magnitude variation of ∼4 mag, the amplitude of the variation is almost an order of magnitude larger than for a typical CLAGN.

We argue that a strong magnitude variation in the *V* or *g* band is not expected for a low-redshift, low-luminosity AGN. First, the optical measurements are probing different parts of the spectral energy distribution. For example, the SDSS-*g* band spans the wavelength range of 4000 to 5400 Å. For MaNGA objects this encompasses the blue end of the spectrum to around the H β region. For the CLAGNs in the MC searches at a mean redshift of 0.3, this bandpass covers the continuum region between H β and Mg II. To probe a similar region to the MC searches, low redshift searches would require near ultraviolet photometry.

Secondly, variations of the H β broad emission line alone will not contribute to a 0.5 mag variation. Assuming a SDSS-*g* band magnitude change of 0.5, this requires that the total flux under the band pass to vary by ∼60 per cent. For an upper limit, if we assume broad H β line FWHM of 4000 km s^{-1}, this corresponds to ∼150 Å in base width, and occupies ∼1/10 of the band pass. Therefore, a six-fold change in H β is necessary for it alone to produce the 0.5 mag variation, which is not possible considering broad H β variation is less than broad H α, and even H α is not known to change in that scale for CLAGNs.

Instead, it is the variation of the AGNs continuum that dominates the observed photometric variation. For the higher redshift CLAGNs in the MC searches, the AGNs continuum dominates the spectrum. This is because, the host galaxy is insignificantly dim. If we compare a host galaxy at redshift 0.5 and another at 0.05, the former is 140 times fainter in luminosity or 5 mag dimmer. High-redshift AGNs that are detectable in surveys therefore have sufficiently high luminosity and dominates all observation. As such, their AGNs continuum variation can be observed. For our case of low-redshift CLAGNs, the spectra is still dominated by the host galaxy continuum as galaxy absorption features around 4000 Å are still present. Furthermore these absorption lines do not disappear or change (illustrated by flat profile in relative-change plots) even with the broad lines appearing. This suggests that the AGNs continuum is relatively insignificant to the overall spectra. Therefore, continuum changes is not visible and hence a CLAGN caused magnitude variation at the 0.5 mag level is not possible.

In an attempt to verify this argument, we performed synthetic photometry with the SDSS-*g* band filter on the spectra from our work, as well as those in MC searches. Due to mismatching apertures, equipment and exposure conditions, normalizing spectra is complex. CLAGNs in the MC searches with both SDSS spectra are those least affected by these issues. These produced $\Delta g >$ 0.5 as expected. For the MaNGA sample, two methods were attempted. First, the [O III] flux emission was assumed to remain constant. Secondly, the MaNGA spectra were scaled to account for the aperture differences (divided by 1.36 or 1.56). In both methods, a large spread of magnitude changes were found. In some cases, the continuum showed a large decreasing magnitude with appearance of broad emission lines. Similarly, large systematic errors from comparing spectra were reported in Thomas et al. (2017), where well matched pairs of spectra were taken using the same instrument.

The attempt at synthetic photometry is not successful. None the less, based on the presented arguments, the AGNs continuum has only made a small contribution to our low-redshift spectrum. This suggests that even for 2 arcsec (BOSS fibre diameter), we would not observe AGNs continuum variation as the spectrum is dominated by galaxy light. Thus, CSS and ASAS-SN which use much larger apertures are not useful for the detection of low-redshift CLAGNs. Either a 0.1 arcsec aperture from a space-based telescope less affected by seeing variations or a probe of the near-ultraviolet region where the galaxy continuum no longer dominates, may be required for observable changes.

MIR on the other hand appears to be much more variable for our sources. This includes our sources in the supplementary sample. On one hand, this would suggest that the MIR is better than optical at detecting AGNs variations and consequently the CLAGNs event. This is seen in J0828427+454433 and other known CLAGNs (MC; Sheng et al. 2017; Stern et al. 2018). The MIR is less affected by dust compared to the optical and therefore reveals luminosity changes more accurately. However *WISE* apertures might also be too large to detect the AGNs continuum variation. Furthermore, the MIR response of CLAGNs in those referred work appears inconsistent with light curves that either correlates, anticorrelates, or no correlation to the optical, and all with varying time-delays. As such, we cannot confidently attribute the observed variations to the AGN, until the CLAGNs spectral energy distribution at the MIR is understood.

4.2 The supplementary sample

These are objects where we detect a signature of change in the broad lines, but they were discarded as they do not fit the typical CLAGNs phenomena for various reasons. This means that these are highly variable AGNs that are still interesting to discuss. Heres we present their light curves in Fig. 7, spectra in Figs 4 and 5. The line-fitting results for four of the objects are presented in Table 2. J0752441+455657 is a special case and is presented in Table 3.

4.2.1 Strong H α changes only

Three objects, J0745072+460420, J0756437+445124, and J2107219+110359 were initially selected for their signatures of broad-line changes in the divided spectra for broad H α emission line and H β albeit to a lesser degree. These are presented in Fig. 4. In all three, both MaNGA and SDSS spectra of the broad H β emission line are not observable visually or through line fitting. From both BPT diagrams, J0756437+445124 and J2107219+110359 are likely AGNs, and they would be type 1.9. While in both cases the H α broad emission line luminosity decreased by ∼70 per cent, there is no change in type classification and we do not consider them CLAGNs. *WISE* and ASAS-SN light curves show that J2107219+110359 is steadily decreasing in luminosity, thus, we encourage further observations as we might see the H α broad line vanishing completely, hence a type 1.9 to type 2 CLAGN. Meanwhile, the *WISE* and ASAS-SN light curves for J0756437+445124 taken after the MaNGA spectrum are highly variable or noise dominated around a mean, thus, not very informative. However, a future spectra to check the presence of H α is still encouraged.

J0745072+460420, on the other hand, is a possible AGN and a likely LINER according to the BPT diagrams. However, unlike the LINER J1605051+452634, the *W1–W2* colour is much bluer and atypical of an AGN. This suggests that the AGNs activity may have ceased or be non-existent, meaning that the variation is not caused by AGNs activity. However, the decrease in H α broad emission line luminosity is at ∼70 per cent. Such large variations are on par with CLAGNs. Then again, unlike the known Changing Look LINER galaxies, this object lacks broad H β variations. CRTS and *WISE*

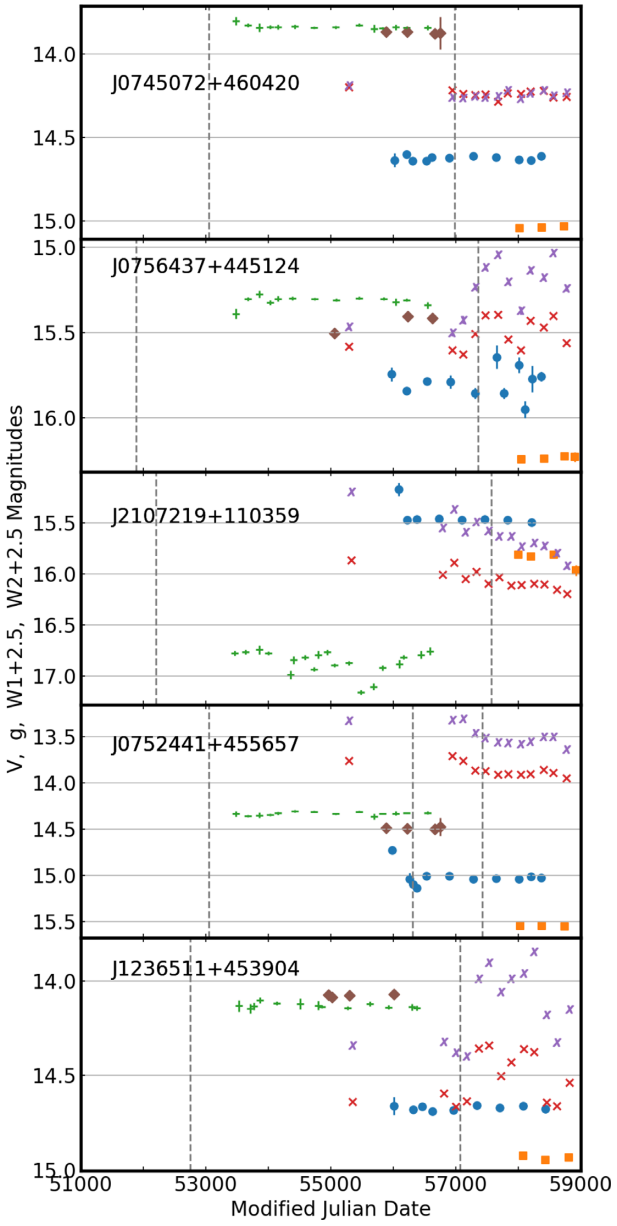

Figure 7. Axes and points same as Fig. 6.

light curves reveal the possibility of a small decrease in magnitude in the past. Perhaps MaNGA observed the object close to the end of a ∼10 yr time-scale variation. A future spectrum could see the broad lines disappearing completely.

4.2.2 J0752441+455657

This object is likely to be considered as a LINER based on the BPT diagrams. It was initially selected for the magnificent three trough features in both the H α and H β broad emission line observed in the division spectrum. The three trough feature corresponds to a multicomponent broad absorption-line system. From measuring the peaks of the trough, we find a redshift of 0.0332 for the redward trough, and 0.0704 for the blueward trough. The time between the SDSS and BOSS spectra is 9 yr and between BOSS and MaNGA is a ∼1000 d. The short time period between the latter suggests that the variations of this object are atypical of an AGN. However, multicomponent variations are also atypical of CLAGNs, therefore we are not sure if the observed variations are caused by a Changing Look event or another phenomenon.

While there is a suggestion of a P-Cygni profile with the absorption like feature at 6497 Å, we cannot be certain if the feature is indeed a P-Cygni profile, or a metal absorption-line feature, or a feature shaped by two broad emission lines. We shall assume the last as the nature of this absorption does not change the presence of a multicomponent broad-line system. The relative change plot of MaNGA/BOSS shows strong variations in all three components of the H α broad line, while the plot of MaNGA/SDSS only has significant variation for the central region. This suggests that the object is close to its peak bright stage during the BOSS spectrum.

During line fitting, we separate this system into the centre, blue and red components, and report their measured flux, FWHM, and centroid in detail in Table 3. We could only line fit the H α region as H β is hidden.

For the centre broad emission line, we observe a 74 per cent decrease in emission-line luminosity for H α and a ∼3 per cent decrease in normalized flux for the corresponding H β component according to the relative-change plot. The FWHM of this component decreased by ∼800 km s^{-1}, while the centroid remains roughly unchanged.

For the blue broad emission line, the spectral profile has spread out with an ∼4000 km s^{-1} increase in FWHM. As a result, there is a 54 per cent increase in emission-line luminosity, even though the strength of the peak is now much lower. The centroid has also shifted redward by ∼25 km s^{-1} that could suggest a deceleration of the emitter. A decrease of ∼4 per cent is observed for the corresponding H β component in the relative-change plot.

The red broad emission line is constructed with two Gaussian components. The emission luminosity of H α decreased by 72 per cent, while the normalized flux of the corresponding H β component decreased by ∼8 per cent from the relative-change plot. The emission-line width has also increased by ∼1000 km s^{-1} in FWHM. The emission-line centroid remains roughly unchanged.

The possibility of a P-Cygni profile and the presence of such broad emission lines might suggest that the object is a supernova. Indeed, there is a decrease in 0.3 mag in the *WISE* light curve roughly in between the two spectra that could be consistent with a light curve of a supernova that has an extended fading phase. ASAS-SN *V* band also has a sharp change in magnitude right before the BOSS spectrum, however, this variation is doubtful since PTF and CSS do not show similar behaviour. Future observations would certainly be helpful in understanding the nature of this object.

4.2.3 J1236511+453904

The classification of this object is not clear. The spectral morphology indicates a Narrow Line Seyfert 1 (NLS1). However, it is possible to fit the emission features with only intermediate-width (1000 > FWHM > 2000 km s^{-1}) Gaussian curves, and also with broad and narrow lines. Fitted broad lines have a mean FWHM of ∼2500 km s^{-1} except for the broad H β of the SDSS spectrum. Here, the resulting FWHM is ∼1700 km s^{-1}, thus favouring an NLS1. The two methods also produce consistent total emission-line fluxes except for the H α region of the MaNGA spectrum, where the spectral feature favours the 'broad and narrow line' method. Therefore, the line-fitting results do not provide a clear distinction.

The BPT diagram places this object in the AGN and borderline LINER class. We do not consider it as a CLAGN as first, we are not

Table 2. Similar to Table 1. Table consists of line-fitting results of the three objects with H α only change and one that we suspect to be a Narrow Line Seyfert 1 (NLS1). We exclude broad H β and consequently broad/narrow H β as it is irrelevant to the first three objects. An additional row is presented for J1236511+453904, which is the NLS1 suspect. This is due to the possibility of the emission-line profiles to be fitted with a broad line (see Section 4.2.3). The values in the brackets are the broad-line components. Adding up the values is consistent with the result from fitting the emission-line feature with a single intermediate width emission line (1000 < FWHM < 2000 km s^{-1}).

	J0745072+460420		J0756437+445124		J2107219+110359		J1236511+453904	
	SDSS	MaNGA	SDSS	MaNGA	SDSS	MaNGA	SDSS	MaNGA
MJD	53055	56980	51883	57363	52207	57572	52753	57073
$F_{\mathrm{H}\beta,\mathrm{narrow}}/F_{[\mathrm{OIII}]}$	–	–	0.093	0.079	0.265	0.168	0.091 (+ 0.604)	0.089 (+ 0.224)
$L_{\mathrm{H}\alpha,\mathrm{broad}}(10^{40} ergs/s)$	3.422	1.565	4.113	2.086	6.889	1.545	7.345	4.287
$\Delta L_{\mathrm{H}\alpha,\mathrm{broad}}$	54.27 per cent		49.27 per cent		77.58 per cent		41.64 per cent	
Derived type	LINER	LINER	1.9	1.9	1.9	1.9	NLS1?	NLS1?
Redshift	0.0309		0.0499		0.0425		0.0303	
RA, Dec.	116.2802, 46.0724		119.1822, 44.8567		316.8413, 11.0664		189.2133, 45.6512	

Table 3. Line-fitting results for J0752441+455657. The separated H α entry at the bottom of the table refers to the multi-component broad lines. The measurements presented here for MaNGA are from spectrum extracted with a 2-pixel radius aperture that is most similar to the BOSS spectrum. Note that the fitting parameters depend on the initial assumption of having a multicomponent broad-line system. Since the H α region is large with broad structures, the fitting procedure is complex. Small changes will greatly alter the fitting results. As such acquiring a measurement uncertainty is not practical. From previous testing of the line-fitting algorithm, we find a consistent upper limit of 5 per cent error for all measured values.

	Relative flux $F_x/F_{[\mathrm{OIII}]}$			FWHM (km s^{-1})			Centroid (Å)		
LINES	SDSS	BOSS	MaNGA	SDSS	BOSS	MaNGA	SDSS	BOSS	MaNGA
[O I]	0.571	0.474	0.510	571.335	668.415	543.232	6302.301	6301.409	6301.826
[N II] 6585.27 Å	0.955	0.794	0.929	486.049	383.776	389.892	6585.024	6585.014	6585.203
[N II] 6549.86 Å	0.251	0.226	0.183	427.631	450.235	304.922	6549.017	6548.511	6549.068
[S III]	0.534	0.481	0.470	415.942	625.621	677.966	6733.054	6732.433	6732.598
H α	0.213	0.148	0.150	426.589	320.840	260.756	6565.020	6563.954	6564.283
H α Centre	3.176	4.185	2.927	3843.201	4044.310	3215.527	6558.352	6561.146	6565.234
H α blue	0.956	1.479	2.124	3593.723	3264.235	7223.609	6456.998	6451.636	6476.797
H α red	1.066	4.292	3.157	4921.205	6491.280	7517.084	6666.374	6683.293	6679.346
		Redshift			RA, Dec.			MJD	
		0.0516			118.1842, 45.9493		53055	56309	57428

sure of its classification. Secondly, there is no type change, assuming the emission lines are broad. Thirdly, assuming that it is an NLS1, no Changing Look NLS1 has been discovered to date. However, the object has strong variations across all emission lines and absorption lines. This includes the decrease in flux of the Balmer series, He II and He I emission lines, and the appearance of the H absorption line. Furthermore, He II emission line appears to have lost a broad-line component. We also see strong variations in the *WISE* light curves, with fluctuations of ∼0.3 mag for *W1* and ∼0.5 for *W2*, which could be caused by noise. However the MaNGA spectrum that corresponds to a dimmer stage, is taken at a dim period of the *WISE* light curves. It is possible that the MIR fluctuations are real, strongly reflecting the object's variability. Future observations, to verify this and to determine whether the object is indeed a Changing Look phenomena, are encouraged.

5 SUMMARY

Using SDSS and MaNGA spectra from SDSS DR15, we performed a blind CLAGNs search over 438 MaNGA spectra and discovered four new CLAGNs, one of which, J1605051+452634 is a Changing Look LINER. Due to the lack of accurate spectral classification in the SDSS data base, we expect the true number of AGNs in this sample to be fewer than 400. This results in a lower limit for our CLAGNs rate of ∼1 per cent that is in the same order as the rates found in Wolf et al. (2018) and Runco et al. (2016). However, our search only involves the AGNs sample with true positive and false positives classified by the SDSS automated spectral classifier. We expect more CLAGNs to be found within the false negatives among the remaining 4 183 galaxies.

We could only place upper limits on change time-scales from the spectral epochs. These range from ∼ 3 to 15 yr. In three of our objects (with the exception of J0828427+454433), we find continuing variability in the light curves. Newer spectra for these objects could be informative for CLAGNs.

In addition, we also find five highly variable objects. Two of which (J0756437+445124 and J2107219+110359) are type 1.9 AGNs with variations only in H α and further evolution leading to a type 2 AGNs is possible. One (J0745072+460420) is a LINER type galaxy with changes that could be consistent with a changing look LINER. One (J1236511+453904) is an NLS1 with strong MIR variations that might indicate future emission-line changes. Finally, the last object (J0752441+455657) has a three component broad line in H β and H α with strong variations, which we have little understanding of. Newer spectra for all of these will be useful for other highly variable events and even possibly for CLAGNs.

None of our CLAGNs satisfy the selection threshold for > |0.5| optical magnitude variability that has been successful in other CLAGN searches (MC searches and Wolf et al. 2018). Therefore, the selection threshold is not effective in the range of redshifts that we are probing. This is because, the frequently used *g* band is situated in a different section of the AGNs spectral energy distribution.

Furthermore, at low redshifts, the galaxy continuum dominates the spectrum and overwhelming the AGNs continuum. Therefore, ground-based optical photometry which utilizes a large aperture will not be able to detect the variation caused by the CLAGNs event. We plan to examine the near ultraviolet region for CLAGNs in the future.

W1 and *W2* from *WISE* appear to be more sensitive to CLAGNs variation than optical data. While MIR viability in finding CLAGNs has been known, the correlation between MIR magnitude changes and the CLAGNs event has yet to be physically understood. We intend to explore the MIR for CLAGNs in a future work as well.

Most of the CLAGNs known to date have changed in the past (MC) since they were found in searches within pre-existing databases. However this restricts the study of CLAGNs, as we are investigating a dynamical process with only limited data in the past. Having continuous data across the period of change is extremely powerful as demonstrated by the CLAGN found in Trakhtenbrot et al. (2019) and Oknyansky et al. (2018). Therefore, a shift in paradigm in how we look for CLAGNs is required. Future data sets, such as optical light curves from The Vera C. Rubin Observatory Legacy Survey of Space and Time (LSST) Survey and time-series spectroscopy from SDSS-V, will be invaluable resources for CLAGNs studies.

ACKNOWLEDGEMENTS

WJH would like to thank the University of Melbourne for an International Graduate Research Scholarship. Funding for the Sloan Digital Sky Survey IV has been provided by the Alfred P. Sloan Foundation, the U.S. Department of Energy Office of Science, and the Participating Institutions. SDSS-IV acknowledges support and resources from the Center for High-Performance Computing at the University of Utah. The SDSS web site is www.sdss.org. SDSS-IV is managed by the Astrophysical Research Consortium for the Participating Institutions of the SDSS Collaboration. The CSS survey is funded by the National Aeronautics and Space Administration under Grant No. NNG05GF22G issued through the Science Mission Directorate Near-Earth Objects Observations Program. The CRTS survey is supported by the U.S. National Science Foundation under grants AST-0909182 and AST-1313422. The ASAS-SN survey is partially funded by Gordon and Betty Moore Foundation with a 5-yr grant GBMF5490. The team is also supported by NSF Grants AST-151592 and AST-1908570. The survey telescopes are hosted by LCO global. ASAS-SN expansion was also possible with support from: Peking University, Mt. Cuba Astronomical Foundation, OSU Center for Cosmology and AstroParticle Physics (CCAPP), the Chinese Academy of Science South America Center for Astronomy (CAS-SACA), and the Villum Foundation (Denmark). This publication makes use of data products from the Near-Earth Object Wide-field Infrared Survey Explorer (*NEOWISE*), which is a project of the Jet Propulsion Laboratory/California Institute of Technology. *NEOWISE* is funded by the National Aeronautics and Space Administration. We greatly appreciate Katie Auchettl and Michele Trenti from the University of Melbourne for comments in improving the manuscript. We are also grateful to the referee for helpful suggestions.

DATA AVAILABILITY

The datasets were derived from sources in the public domain: CASJOB at https://skyserver.sdss.org/CasJobs/, and LAMOST at http://dr5.lamost.org/.

REFERENCES

Aghanim N. et al., 2018, preprint (arXiv:1807.06209)
Aguado D. S. et al., 2019, ApJ, 240, 23
Bischoff K., Kollatschny W., 1999, A&A, 345, 49
Bundy K. et al., 2014, ApJ, 798, 7
Cappellari M., 2016, MNRAS, 466, 798
Cohen R. D., 1983, ApJ, 273, 489
Cohen R. D., Puetter R. C., Rudy R. J., Ake T. B., Foltz C. B., 1986, ApJ, 311, 135
Dawson K. S. et al., 2012, AJ, 145, 10
Denney K. D. et al., 2014, ApJ, 796, 134
Drake A. J. et al., 2009, ApJ, 696, 870
Eisenstein D. J. et al., 2011, AJ, 142, 72
Flewelling H. A. et al., 2016, preprint (arXiv:1612.05243)
Frederick S. et al., 2019, AJ, 883(1), 31
Husemann B. et al., 2016, A&A, 593, L9
Kauffmann G. et al., 2003, MNRAS, 346, 1055
Kewley L. J., Dopita M. A., Sutherland R. S., Heisler C. A., Trevena J., 2001, ApJ, 556, 121
Kewley L. J., Groves B., Kauffmann G., Heckman T., 2006, MNRAS, 372, 961
Kochanek C. S. et al., 2017, PASP, 129, 980
LaMassa S. M. et al., 2015, ApJ, 800, 144
Law N. M. et al., 2009, PASP, 121, 1395
MacLeod C. L. et al., 2016, MNRAS, 457, 389
MacLeod C. L. et al., 2019, ApJ, 874, 8
Mainzer A. et al., 2011, AJ, 731, 1
Nascimento J. C. D. et al., 2019, MNRAS, 486, 5075
Oknyansky V. L., Winkler H., Tsygankov S. S., Lipunov V. M., Gorbovskoy E. S., van Wyk F., Buckley D. A. H., Tyurina N. V., 2019, MNRAS, 483, 558
Osterbrock D. E., 1981, ApJ, 249, 462
Penston M. V., Perez E., 1984, MNRAS, 211, 33P
Ross N. P. et al., 2013, AJ, 773, 27
Ruan J. J. et al., 2016, ApJ, 826, 188
Ruan J. J., Anderson S. F., Eracleous M., Green P. J., Haggard D., MacLeod C. L., Runnoe J. C., Sobolewska M. A., 2019, preprint (arXiv:1909.04676)
Runco J. N. et al., 2016, AJ, 821, 33
Shappee B. J. et al., 2014, ApJ, 788, 48
Sheng Z., Wang T., Jiang N., Yang C., Yan L., Dou L., Peng B., 2017, AJ, 846, L7
Stern D. et al., 2018, ApJ, 864, 27
Thomas A. D. et al., 2017, ApJS, 232, 11
Tohline J. E., Osterbrock D. E., 1976, ApJ, 210, L117
Trakhtenbrot B. et al., 2019, ApJ, 883, 10
Wake D. A. et al., 2017, AJ, 154, 86
Wisotzki L., Koehler T., Groote D., Reimers D., 1996, A&A, 115, 227
Wolf C., Onken C. A. et al., 2018, PASA, 35, 29
Wright E. L. et al., 2010, AJ, 140, 1868
Wylezalek D., Zakamska N. L., Greene J. E., Riffel R. A., Drory N., Andrews B. H., Merloni A., Thomas D., 2018, MNRAS, 474, 1499
Yang Q. et al., 2018, ApJ, 862, 109
Yanny B. et al., 2009, AJ, 137, 4377

APPENDIX: DIVISION SPECTRA OF THE FOUR CLAGN CANDIDATES AND SOME EXAMPLES

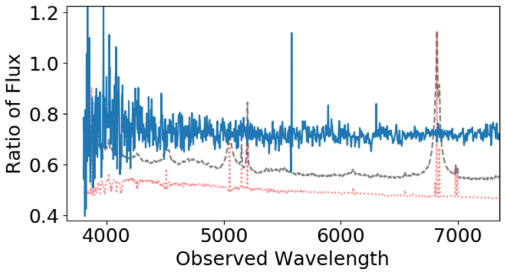

Figure A1. Example of ratio spectrum with no changes.

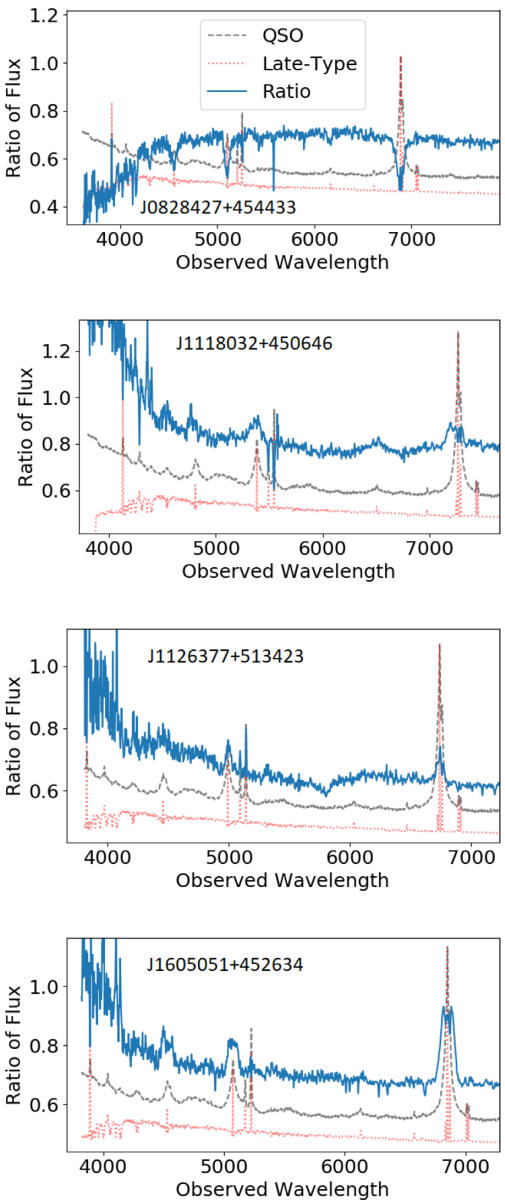

Figure A2. Our objects all with clear broad-line changes.

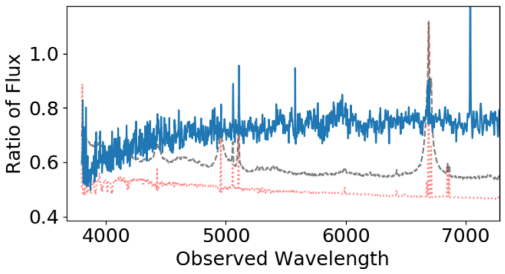

Figure A3. Example of ratio spectrum with only narrow changes.

This paper has been typeset from a TEX/LATEX file prepared by the author.